Paleomagnetism in Extremadura (Central Iberian zone, Spain) Paleozoic rocks: extensive remagnetizations and further constraints on the extent of the Cantabrian orocline

Daniel Pastor-Galán, Gabriel Gutiérrez-Alonso, Mark J. Dekkers & Cor G. Langereis

Journal of Iberian Geology
Including Latin America and the Mediterranean

ISSN 1698-6180
Volume 43
Number 4

J Iber Geol (2017) 43:583-600
DOI 10.1007/s41513-017-0039-x

Springer

J Iber Geol (2017) 43:583–600
https://doi.org/10.1007/s41513-017-0039-x

RESEARCH PAPER

Paleomagnetism in Extremadura (Central Iberian zone, Spain) Paleozoic rocks: extensive remagnetizations and further constraints on the extent of the Cantabrian orocline

Daniel Pastor-Galán[1] · Gabriel Gutiérrez-Alonso[2,3] · Mark J. Dekkers[4] · Cor G. Langereis[4]

Received: 5 June 2017 / Accepted: 14 October 2017 / Published online: 2 November 2017

Abstract
Introduction The winding Variscan belt in Iberia, featuring the Cantabrian orocline (NW Iberia) and the Central Iberian curve, is a foremost expression of the late Carboniferous amalgamation of Pangea, which produced remagnetizations spanning almost the entire globe.
Geological settings Also in Iberia, late Carboniferous remagnetizations are widespread often hindering paleomagnetic interpretations in terms of pre-Pangean geologic history. In contrast, such remagnetizations facilitated the kinematic study of the Cantabrian orocline. Immediately to its south is located the Central Iberian curve whose geometry and kinematics are under debate. Recent studies suggest that this putative structure cannot have formed in the same process as the Cantabrian orocline.
Results Here we present a paleomagnetic and rock magnetic study from Extremadura, a region in the utmost west of the southern limb of the Central Iberian curve. Our new results show two distinct remagnetization events in Paleozoic rocks in Extremadura: (1) Mesozoic or Cenozoic remagnetization occurring in dolomitized limestones and (2) late Carboniferous remagnetization in limestones, characterized by consistent shallow inclinations, but largely scattered declinations indicating a counter clockwise (CCW) vertical axis rotation. Pyrrhotite is documented as magnetic carrier in the limestones which testifies a remagnetization under anchimetamorphic conditions, i.e. during the Variscan orogeny.
Interpretation We interpret the declination scattering as a remagnetization coeval to the vertical axis rotation. The described CCW rotations are those expected for the southern limb of the Cantabrian orocline and are in disagreement with a late Carboniferous secondary origin for the Central Iberian bend, extending the Cantabrian orocline to at least most of the Iberian peninsula.

Keywords Paleomagnetism · Central Iberian zone · Remagnetization · Cantabrian orocline · Carboniferous tectonics

Resumen
Introducción El orógeno Varisco, que en la península Ibérica está curvado y contiene el Oroclinal Cantábrico (NO de Iberia) y la curva orogénica Centro Ibérica, es el resultado más visible de la amalgamación de Pangea en el Carbonífero superior. Durante ese tiempo, la formación de Pangea produjo remagnetizaciones en todos los continentes. En Iberia, las remagnetiaciones del Carbonífero superior son muy extensas y afectan a casi todas las rocas ocultando y dificultando cualquier interpretación paleomagnética de la historia geológica anterior al Pérmico. Paradójicamente, dichas remagnetizaciones facilitaron el estudio de la cinemática del Oroclinal Cantábrico. Inmediatamente al sur de este oroclinal se sitúa la curva

Electronic supplementary material The online version of this article (doi:10.1007/s41513-017-0039-x) contains supplementary material, which is available to authorized users.

✉ Daniel Pastor-Galán
dpastorgalan@gmail.com

[1] Center for North East Asia Studies, Tohoku University, 41 Kawauchi, Aoba-ku, Sendai 980-8576, Japan

[2] Departamento de Geología, Universidad de Salamanca, Pza. de los caídos s/n, 37008 Salamanca, Spain

[3] Geology and Geography Department, Tomsk State University, Lenin Street 36, Tomsk, Russian Federation 634050

[4] Paleomagnetic Laboratory "Fort Hoofddijk", Department of Earth Sciences, Universiteit Utrecht, Budapestlaan 17, 3584, CD, Utrecht, The Netherlands

orogénica Centro Ibérica cuya geometría y cinemática están bajo debate. Algunos estudios recientes apuntan a la posibilidad de que la curva Centro Ibérica se formase a la vez que el Oroclinal Cantábrico.

Resultados En este artículo presentamos los resultados paleomagnéticos obtenidos rocas Paleozoicas de Extremadura, región que contiene la sección sur-occidental de la curva Centro Ibérica. Nuestros resultados muestran dos remagnetizaciones separadas en el tiempo: 1) Una remagnetizaciión Mesozoica o Cenozoica que aparece en calizas dolomitizadas y 2) Una remagnetización del Carbonífero tardío cuyas características incluyen inclinaciones subhorizontales y declinaciones dispersas que indican una rotación de eje vertical en sentido horario. Además, hemos identificado pirrotina como mineral magnético en las calizas. Este mineral solo aparece en calizas remagnetizadas durante metamorfismo de bajo grado (anquizona).

Discusión Interpretamos que la dispersión en la declinación registra una remagnetización que ocurrió a la vez que la rotación de ejes verticales. La rotación horaria que sugieren nuestros resultados coincide con la esperada para el flanco sur del Oroclinal Cantábrico. Estos resultados contradicen la posibilidad de que la curva Centro Ibérica y el Oroclinal Cantábrico ocurriesen al mismo tiempo y con carácter secundario respecto a la orogenia Varisca, y extienden las rotaciones de eje vertical ligadas al Oroclinal Cantábrico a todo el sur oeste de la Península Ibérica.

Palabras clave Paleomagnetismo · Zona Centro-Ibérica · remagnetización · Oroclina Cantábrico · Tectónica del Carbonífero

1 Introduction

Remagnetizations are ubiquitous in most orogens on Earth, from the Alps (e.g. Pueyo et al. 2007) to the Himalayas (e.g. Huang et al. 2017) and the Rocky Mountains (e.g. Enkin et al. 2000). In a remagnetized rock, the original natural remanent magnetization (NRM) is replaced or overprinted due a set of geologic processes acting alone or in concert. Although sometimes disregarded because of the implied information loss—the rock record before the orogenesis cannot be recovered-, remagnetized rocks have proven to be an excellent tool to unravel orogenic kinematics., They are capable of constraining vertical axis rotations (e.g. Gong et al. 2009; Izquierdo-Llavall et al. 2015) or evaluating subsequent deformation phases coeval to or postdating the remagnetization event (e.g. Calvín et al. 2017). Remagnetized rocks, therefore, remain as an important source of useful geological information.

The final amalgamation of Pangea during the late Paleozoic Variscan–Alleghanian orogeny is widely recognized as having caused global-scale remagnetizations (e.g. Stamatakos et al. 1996; Zegers et al. 2003; Elmore et al. 2012). In the Iberian peninsula the studies of the widespread late Carboniferous remagnetizations (e.g. Weil and van der Voo 2002; Tohver et al. 2008) were crucial to constrain the kinematics of the Cantabrian "arc", a strongly bent section of the Variscan orogen in Northern Iberia interpreted as a secondary orocline (Hirt et al. 1992; van der Voo et al. 1997; Weil et al. 2000, 2001, 2013; Weil 2006). More recently, the late Carboniferous remagnetizations delivered pivotal input for Pastor-Galán et al. (2015a, 2016) and Fernández-Lozano et al. (2016) to discuss and discard a coeval secondary origin for the alleged curvature in Central Iberia (e.g. Martínez Catalán 2011; Shaw et al. 2012). The extent and boundaries of the Cantabrian orocline are now considered to include the two Paleozoic continents, Gondwana and Laurussia (Pastor-Galán et al. 2015b), involved in the Carboniferous Variscan collision in western Europe.

In this paper we investigate the paleomagnetism and rock magnetism in rocks from Extremadura (southern Central Iberian zone), which provide new insights into the expression of the late Carboniferous remagnetization event in the Iberian hinterland of the Variscan orogen. In addition, our results help to further constrain the extent and kinematics of the Cantabrian orocline and its relationship with the putative Central Iberian curve and assess the extensive hydrothermal activity occurred in Iberia during post-Paleozoic times.

2 Geological background

The collision between Laurussia and Gondwana and several microplates resulted in the late Paleozoic orogen in central and western Europe, known as the Variscan orogen (e.g. Nance et al. 2010). The earliest record of Variscan deformation in Iberia dates ca. 400 Ma (e.g. Dallmeyer and Ibarguchi 1990; Gómez Barreiro et al. 2006), while the continent–continent collision ocurred later, at ca. 365–370 Ma (e.g. Dallmeyer et al. 1997; López-Carmona et al. 2014). At 325–318 Ma, NW Iberia was extensively intruded by anatectic leucogranites and granodiorites, often interpreted as a product of extensional collapse (e.g. Bea et al. 2006; Castiñeiras et al. 2008; López-Moro et al. 2017). From 310 to 295 Ma the originally quasi-linear Variscan orogen buckled around a vertical axis forming the Cantabrian orocline (a.k.a. Ibero-Armorican Arc; Gutiérrez-Alonso et al. 2012; Weil et al. 2013; and references therein). Many sources of geological information support the aforementioned kinematics: paleomagnetic (Weil et al. 2001, 2010), structural (Merino-Tomé et al. 2009; Pastor-Galán et al. 2011, 2014; Shaw et al. 2016), and

geochronological data (Gutiérrez-Alonso et al. 2015a). Petrologic and isotopic data also indicate that a pulse of magmatic and tectonothermal took place over a short time window of 10–15 Myr together with orocline buckling at the end of the Carboniferous (Gutiérrez-Alonso et al. 2011a, b). Orocline formation and large scale intrusions are thought to be part of a single process of lithospheric buckling leading to lithospheric mantle foundering and replacement (Fernández-Suárez et al. 2002; Gutiérrez-Alonso et al. 2004; Pastor-Galán et al. 2012a).

Since the early twentieth century, several authors observed another arcuate structure in the central part of the Iberian Massif, of similar magnitude but with an opposite alleged curvature to the Cantabrian orocline (Staub 1926; Aerden 2004; Martínez-Catalán et al. 2011; Shaw et al. 2012). Its shape, kinematic and tectonic implications remained ignored for several decades, primarily due to poor outcrop exposure (Martínez Catalán et al. 2015). Martínez-Catalán (2011) and Shaw et al. (2012, 2016) hypothesized a common origin for both Cantabrian and Central Iberian curvatures that would have buckled together as coeval secondary oroclines. In contrast, Pastor-Galán et al. (2015a, 2016, in press) performed paleomagnetic studies and presented structural data from the hinge and southern limb of the putative Central Iberian curve that discard a coeval secondary formation for the Cantabrian orocline and Central Iberian curve and suggest that the Central Iberian curve, if real, must have been generated previous to 318 Ma.

The western Europe Variscan orogen is classically divided into a number of zones based on differences in the lower Paleozoic stratigraphy as well as structural style, metamorphism and magmatism, which broadly correspond to increasing distance from the Gondwanan margin (Lotze 1945; Julivert 1971; Franke 1989; Martínez Catalán et al. 1997, 2003; Ballèvre et al. 2014) towards the Rheic ocean. The study area is located in the southernmost part of the Central Iberian zone (CIZ; Fig. 1), one of the different

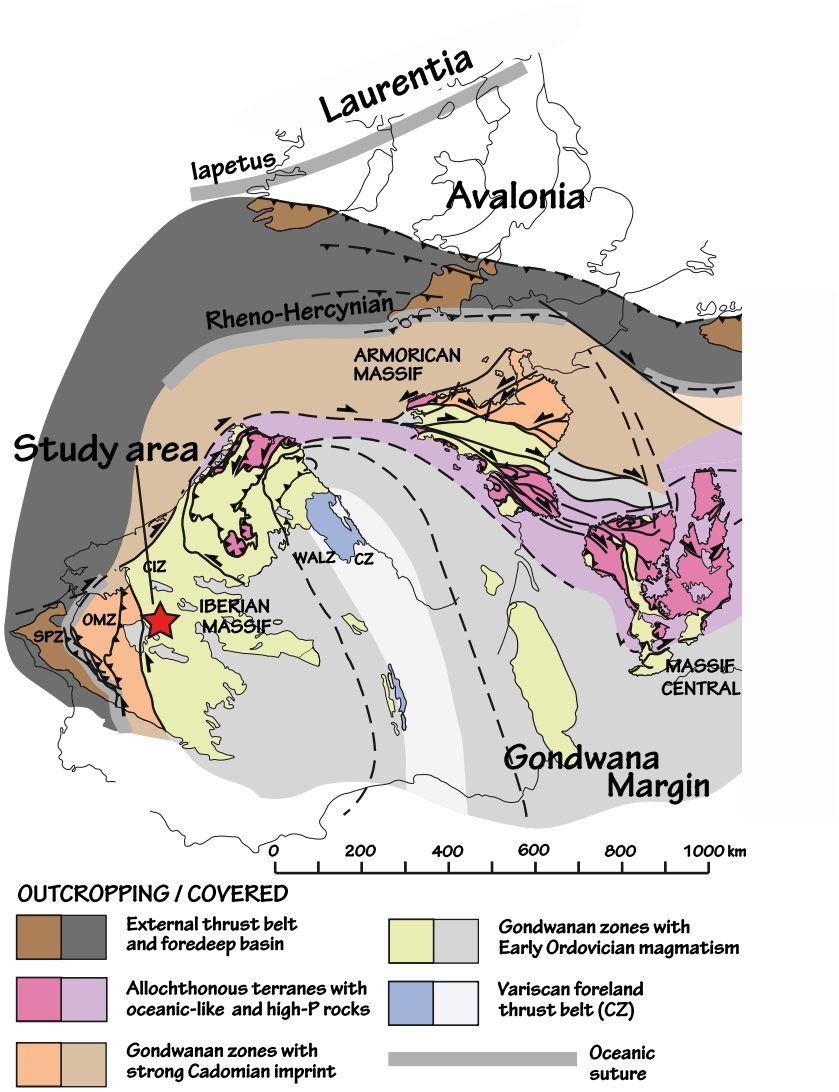

Fig. 1 Permian reconstruction of the West European Variscan Belt (according to Ballèvre et al. 2014, modified by Fernández-Lozano et al. 2016). Red star indicates the location of the study area. *CZ* Cantabrian zone, *WALZ* West Asturian-Leonese zone, *CIZ* Central Iberian zone, *OMZ* Ossa-Morena zone, *SPZ* South Portuguese zone

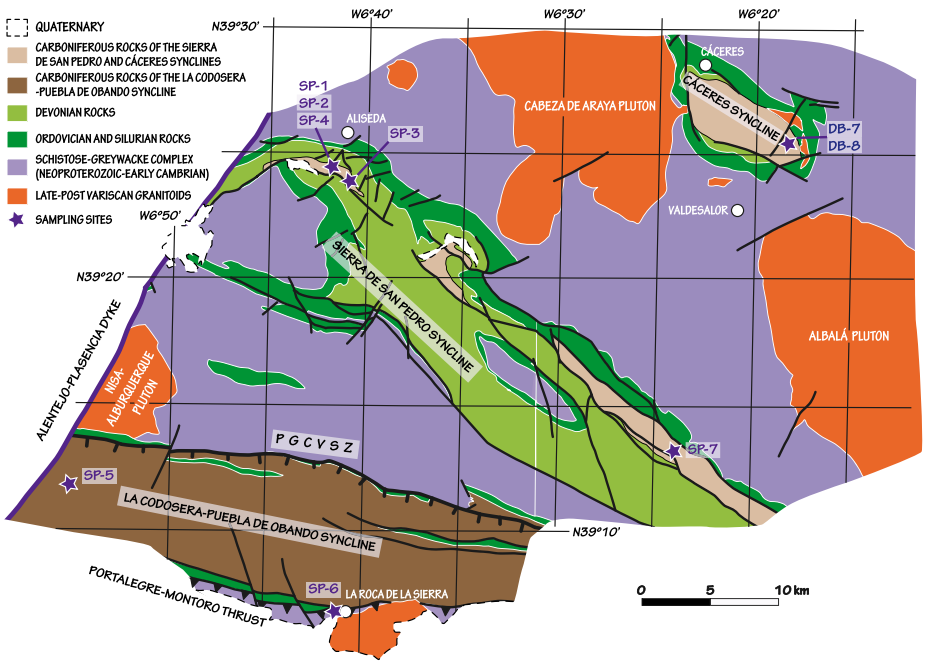

Fig. 2 Geological map of the study area indicating the main structures present in the region and the sampling sites. After (Clariana García et al. 2017) and Matas and Martín Parra (2017)

paleogeographic domains classically described in the Variscan Belt cropping out in Iberia (Lotze 1945; Ballèvre et al. 2014).

The southern CIZ is characterized by a thick sediment sequence of Neoproterozoic to early Cambrian age composed of alternating slates and greywackes (a.k.a. Schist-Greywacke complex). Unconformably overlying it, an up to 4000 m thick Ordovician to Devonian platform passive margin sequence deposited. It consists of alternating slates and quartzites with minor intercalations of volcanic rocks and limestones (e.g. Parra et al. 2006). The succession continues upward with a condensed lower Carboniferous slaty-calcareous unit, which includes intercalations of volcanic tuffs, followed discordantly by late Carboniferous continental conglomerates and sandstones of limited lateral extent (Bochmann 1956; Parra et al. 2006). The stratigraphic sequence terminates with a molassic sequence that postdates the Variscan cycle and was deposited in isolated continental Gzhelian basins (Stephanian in the European geological time scale; e.g., Puertollano; Wallis 1983).

In the southernmost portion of the CIZ, towards its southern border (Fig. 1) at the so called Central Unit (Azor et al. 1994; Simancas et al. 2001), two domains are defined: (i) a narrow outcrop that constitutes the southernmost Allochthonous unit (Martínez Poyatos 2002) composed of mostly Precambrian metasediments, with affinities to the Serie Negra in the Ossa-Morena Unit, overthrusting the (ii) Central Iberian parauthochthonous unit. The Central Iberian parauthochthonous unit is composed of two subunits separated by a major extensional south dipping shear zone named the Puente Génave-Castelo de Vide shear zone (PGCVSZ in Fig. 2; Parra et al. 2006).

In the first of the two domains, the Neoproterozoic Serie Negra includes limestones, which are locally named "Mármoles de la Roca de la Sierra" originally attributed to the Cambrian (Rosso de Luna and Hernández Pacheco 1954) and more recently to the Neoproterozoic. Samples labeled SP6 were retrieved from here. This domain overlains the parauthochthonous through the Portalegre-Montoro Thrust (Fig. 2), emplacing tectonically the Neoproterozoic Serie Negra over the Carboniferous Gévora Formation (Santos and Casas 1979; Soldevila Bartolí 1992a; Rodríguez González et al. 2007). Gévora Fm. crops out in the core of the so-called La Codosera-Puebla de Obando syncline (Santos et al. 1991a, b). Rocks of the Gévora Fm. constitute a siliciclastic sequence with minor interbedded calcareous beds of Visean (Lower Carboniferous) age, based on fossils (Rodríguez González et al. 2007). The sequence is profusely intruded by sills of diabasic-rhyolithic composition. A recent Sm/Nd whole rock study on the diabases has provided an age of 436 ± 17 Ma (López-Moro et al. 2007), which is not in agreement with the paleontological content of their country rocks (Rodríguez González et al. 2007).

In the footwall of the Puente Génave-Castelo de Vide shear zone, in the northern part of the studied region, the CIZ is characterized by a thick sequence of Neoproterozoic-early Cambrian siliciclastic rocks (Schistose-Greywacke complex) unconformably overlain by Ordovician to Carboniferous rocks, mostly siliciclastic, with limestones,

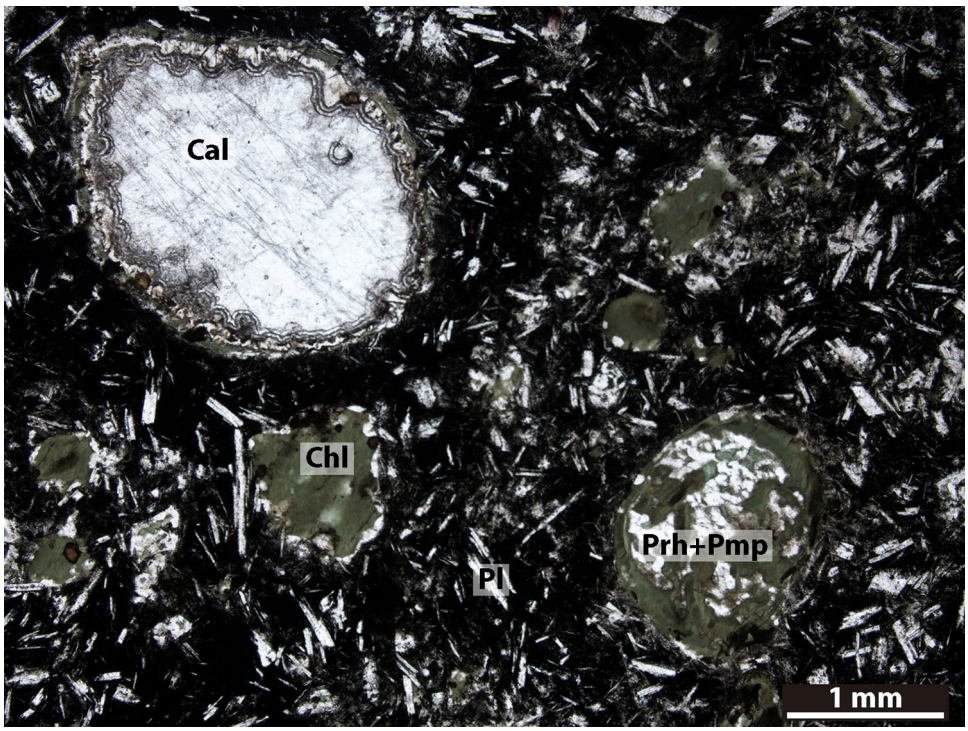

Fig. 3 Microphotograph (plane polarized light) of the lower Carboniferous volcanic rocks in the Sierra de San Pedro syncline where the Prehnite-Pumpellyite association is observed revealing very low grade metamorphic conditions. *Cal* calcite, *Chl* chlorite, *Pl* plagioclase, *Pmp* pumpellyte, *Prh* prehnite

red shales and volcanic tuffs in the lower Carboniferous part. López Díaz (1991), Soldevila Bartolí (1992b), Gutiérrez-Alonso et al. (2015b) provide extensive overviews on the stratigraphy and provenance of the rocks of this sector.

Structurally, in addition to the aforementioned major faults, the studied region is characterized by the presence of large WNW–ESE trending, upright to moderately south-verging, folds (Fig. 2), associated with an axial plane parallel rough cleavage. The rock pile is very-low grade metamorphic (Martínez Poyatos et al. 2001) as evidenced by the presence of chlorite ± prehnite ± pumpellyte associations in the early Carboniferous volcanic rocks in the core of the Sierra de San Pedro syncline (Fig. 3).

Voluminous late- to post-Variscan granitoids are present in the entire region, postdating all the previously described structures. The age of the main granite bodies in the area is ca. 309–305 Ma (U–Pb in zircon) for the Cabeza de Araya Pluton (Fig. 2; Gutiérrez-Alonso et al. 2011a; Rubio Ordóñez et al. 2016) and ca. 306 Ma (U–Pb in zircon) for the Nisa-Albulquerque pluton (Fig. 2; Solá et al. 2009; Gutiérrez-Alonso et al. 2011a).

The CAMP (Central Atlantic Magmatic Province) related Alentejo-Plasencia mafic dyke (NE–SW trend, cf. Fig. 2) was intruded at ca. 200 Ma (Dunn et al. 1998; Rincón et al. 2000; Palencia Ortas et al. 2006). There is no other record of any subsequent tectonic or intrusive effects in the region caused by the Mesozoic Atlantic opening or the Cenozoic Alpine orogeny. Only very minor (up to 3 km) recent strike slip displacements are documented (Villamor 2002).

3 Samples, paleomagnetic results and rock-magnetism

We collected a total of 118 oriented cores with a standard petrol paleomagnetic drill in latest Precambrian to early Cambrian and Carboniferous rocks from nine different sites (labeled SP and DB followed by site number) in Extremadura, W Iberia (Fig. 2, Table 1 and Supplementary file SF1). Samples from sites SP1–SP4, SP7, DB7 and DB8 were retrieved from the hanging-wall of the Puente Génave-Castelo de Vide shear zone whereas SP5 and SP6 were collected in its foot-wall. Sites SP1 to SP4 and SP7 are located in the core of the Sierra de San Pedro syncline, while samples labeled DB came from the Cáceres syncline (Fig. 2). SP1, SP3, SP7 are Lower Carboniferous limestones, DB correspond to equivalent limestones but they are intensely dolomitized. SP2 samples are Carboniferous red fine grained siliciclastic rocks which are stratigraphically immediately below the lower Carboniferous limestones of the Sierra de San Pedro syncline. Finally, samples SP4 are volcanic tuffs and diabases of Lower Carboniferous age cropping out in the core of the Sierra de San Pedro and Cáceres synclines (Corretgé et al. 1982). Samples SP-5 correspond to carbonate layers interbedded into the Gévora Fm. Samples SP6 are also limestones, late Precambrian to

Table 1 N-number of demagnetized specimens

Site name	N	Ns	Cutoff	Geographic		Tilt corrected		R	k	α95	K	A95	A95min	A95max	ΔDx	ΔIx	Coordinates	
				mDec	mInc	mDec	mInc										Longitude	Latitude
SP1	16	17	45	135.2	12.1	108.6	− 49.5	15.6	37	6.1	67.8	4.5	4	14.3	4.5	8.7	− 6.69076	39.40464
SP2	14	14	45	145.7	19.6	136.5	− 49.7	13.6	29.1	7.5	37	6.6	4.2	15.6	6.7	12.1	− 6.69076	39.40464
SP4	12	13	45	139.9	15.5	129.6	− 36	10.4	6.7	18.1	14.2	12	4.4	17.1	12.1	22.6	− 6.69076	39.40464
SP3	8	8	45	127.9	0.4	128.2	− 5.7	7.8	39.6	8.9	61.4	7.1	5.2	22.1	7.1	14.2	− 6.67177	39.38689
SP5	14	15	45	115.2	23.3	11.7	49.2	13.3	18.9	9.4	24	8.3	4.2	15.6	8.5	14.6	− 6.93966	39.18603
SP6	6	9	45	166.4	− 5	80.4	− 79.9	6	151.2	5.5	385	3.4	5.9	26.5	3.4	6.8	− 6.69309	39.11052
SP7	19	19	45	143.9	10.2	152.1	8.4	18.8	73.5	3.9	95.3	3.5	3.7	12.8	3.5	6.8	− 6.40853	39.21550
SP-all geographic	88	95	45	138.3	12.7			82	14.4	4.1	20.6	3.4	2	4.9	3.4	6.6		
SP-all tilt corrected	64	95	45			135.3	− 25.9	54.9	6.9	7.3	11	5.6	2.3	6	5.8	9.6		
DB7	10	13	45	359.9	48.7	10.8	14.3	9.5	17.1	12	13.9	13.4	4.8	19.2	15.5	15.5	− 6.33720	39.44221
DB8	10	10	45	345.1	48.6	354.5	41	9.9	75.3	5.6	57.5	6.4	4.8	19.2	7.4	7.4	− 6.34902	39.44539
DB all geographic	20	23	45	352.4	48.9			19.3	26.5	6.5	20.3	7.4	3.6	12.4	8.6	8.5		
DB all tilt corrected	20	23	45			3.5	28.2	18.7	14.4	8.9	21.5	7.2	3.6	12.4	7.5	12		

Ns number of specimens that passed the Cutoff, *mDec* mean declination, *mInc* mean inclinationg, *k* precision parameter, *α95* radius of the 95% confidence cone about site-mean direction, *K* precision paramenter of the poles, *A95* radius of 95% confidence circle around paleomagnetic pole, *A95min and A95max* describe the minimum and maximun values of A95 allowed to considered the average representative. ΔDx, uncertainty in declination; ΔIx, uncertainty in inclination

early Cambrian in age, intensely strained and recrystallized, that were collected in the southernmost domain of the CIZ.

3.1 Paleomagnetism

The natural remanent magnetization (NRM) of samples was investigated through thermal and alternating field (AF) demagnetization. AF demagnetization was carried out using a robotized 2G-SQUID magnetometer, through variable field increments (4–10 mT) up to 70–100 mT (Mullender et al. 2016). In those samples where pyrite was expected (SP1, SP2, SP4–SP7), we carried out thermal demagnetization up to 350 °C and subsequent AF demagnetization (Fig. 4). This procedure avoids the generation of new magnetite crystals from oxidation of pyrite (usually starting at 400–450 °C; Fig. 5), which precludes proper recovering of the NRM behavior in thermal demagnetization. Stepwise thermal demagnetization was applied with 20–50 °C increments until 350 °C or until complete demagnetization. Some representative vector end-point "Zijderveld" diagrams (Zijderveld 1967) are shown in Fig. 4. A minimum of 5 points were considered to characterize a remanent direction; directions showing maximum angular deviation (MAD) over 15° were discarded. We performed all directional and statistical analyses with the online platform http://www.paleomagnetism.org (Koymans et al. 2016).

Most samples show a low temperature viscous component (VRM), which usually is removed below 200 °C or 15 mT (Fig. 4; Supplementary file SF1). After VRM removal, all samples show a single NRM component generally going to the origin regardless of the different lithologies studied. We identify this component as the characteristic remanent magnetization (ChRM).

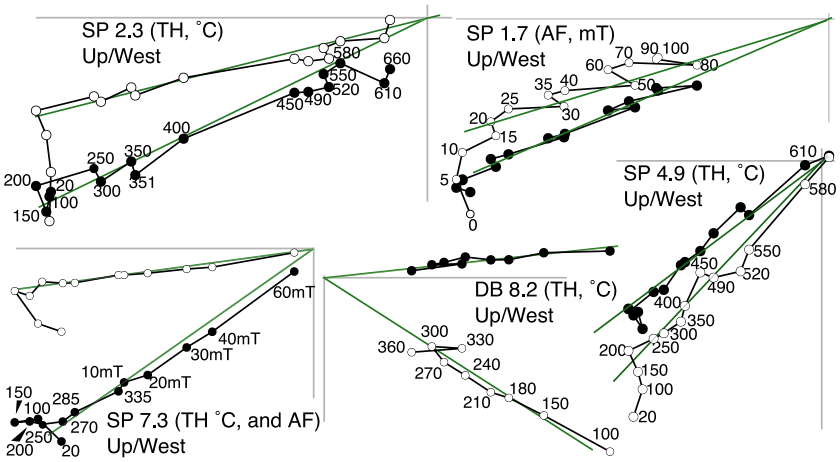

Fig. 4 Examples of vector end-point "Zijderveld" plots and the paleomagnetic directions interpreted from them. Closed (open) symbols represent the projection on the horizontal (vertical) plane

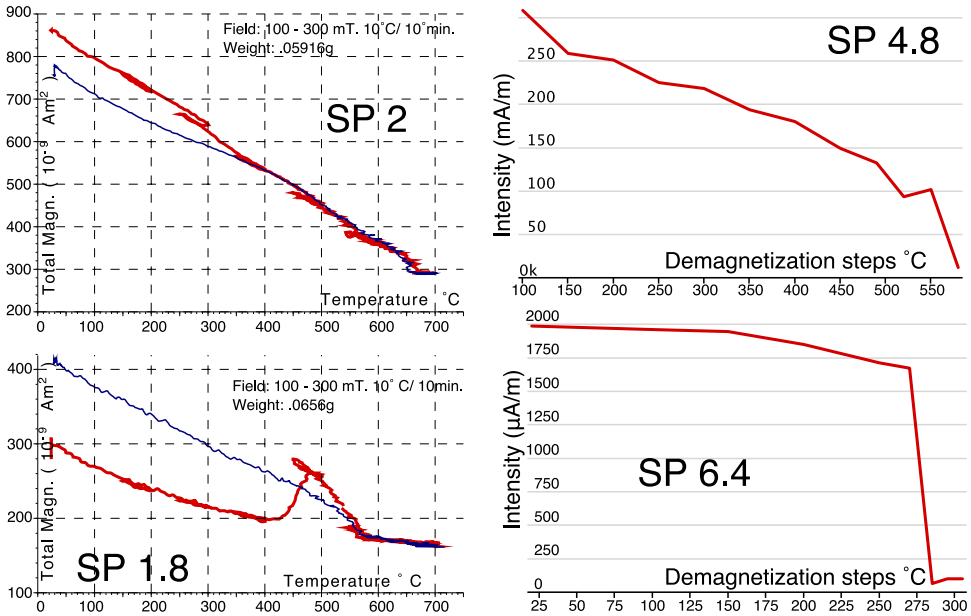

Fig. 5 Thermomagnetic (SP2 and SP1.8) and thermal decay curves (SP4.8 and SP6.4) used to infer the magnetic mineralogy. SP2 (siltstone) reveals the presence of hematite. SP 1.8 (limestone) shows a paramagnetic behavior together with the presence of pyrite (non-magnetic) that transforms into magnetite when the sample is heated over 400 °C. SP4.8 (metavolcanic rock) shows (Ti−) magnetite as the main carrier. SP 6.4 (limestone): main carrier is pyrrhotite

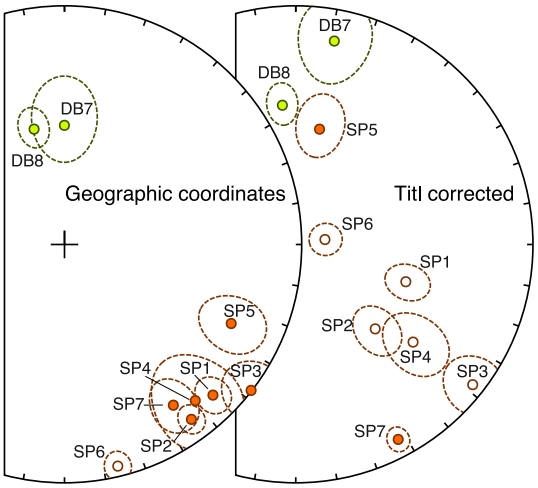

Fig. 6 Equal area stereographic projections showing the mean direction of each site and the projection of their A95. Open points represent upper hemisphere projection

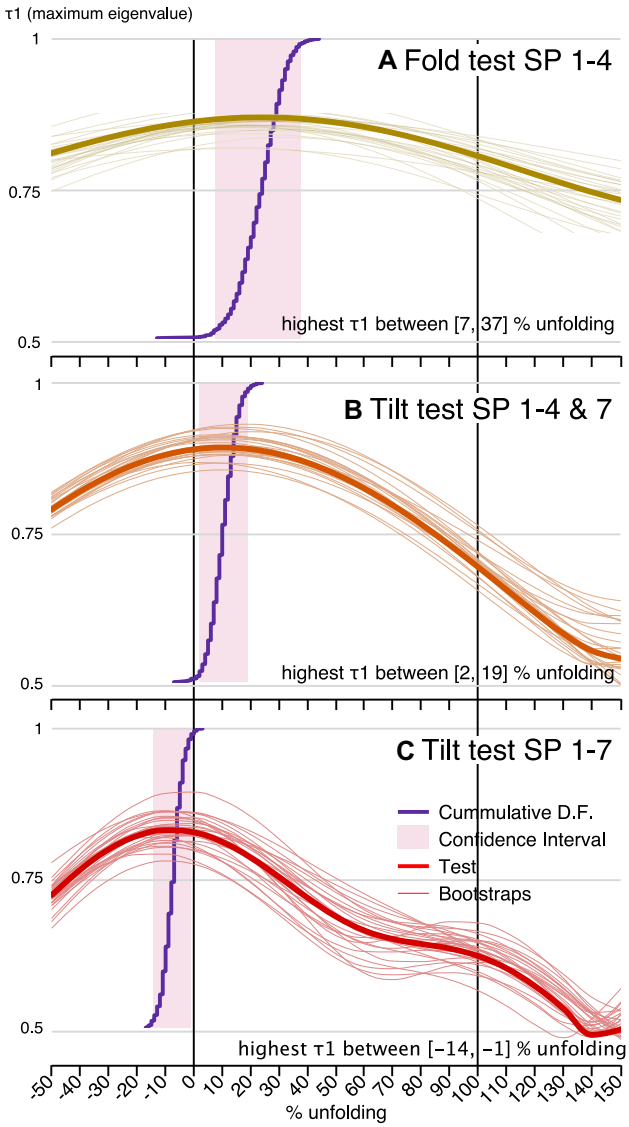

Fig. 7 Negative fold and tilt-tests following Tauxe and Watson (1994) performed in SP samples

Demagnetization analysis of the limestone samples (SP1, SP3, SP5, SP6, SP7) confirms that pyrrhotite and magnetite are carriers of the magnetization in different proportions depending on the site and the individual sample. Some samples are fully demagnetized between 280 and 320 °C and barely demagnetized in AF which is a foremost characteristic of pyrrhotite (Fig. 5; Supplementary file SF1; Dekkers 1988; Pastor-Galán et al. 2016) and others are completely demagnetized at 60 mT or 580 °C which indicates the presence of (low Ti−) magnetite. SP4 (volcanic) and DB (DB7 and DB8, dolomitized limestones) are fully demagnetized at 580 °C and between 60 and 80 mT, indicating that the carrier is magnetite (Fig. 4). The carrier in SP2 samples (red siltstones) is hematite, thermally demagnetizing at temperatures over 600 °C and showing barely any decay during AF demagnetization.

Mean directions and uncertainties of each component were evaluated using Fisher statistics of virtual geomagnetic poles (VGPs). We applied a fixed 45° cut-off to the VGP distributions of each site. In addition, we used the Deenen et al. (2011) criteria to evaluate the scatter of VGPs. As a general rule, if scatter is—mostly—due to paleosecular variation (PSV) of the geomagnetic field, the associated VGP distribution has to be circular. However, structural problems, vertical axis rotation or inclination shallowing may add important sources of scatter. In such cases, VGP distributions will be elongated instead of circular.

ChRM directions in SP and DB samples appear to be different. In SP samples we identified a single polarity NRM component with shallow inclinations (between − 5° and 20°) and declinations ranging from 128° to 166° in geographic coordinates (Table 1; Fig. 6). After tilt correction, site averages show marked scatter (Fig. 6). We performed a fold-test (SP1–SP4) and two tilt-tests in combining this fold test with the rest of SP samples (Fig. 6). A first tilt-test includes SP7 samples collected in the same structural unit (Fig. 7b), but relatively far from the syncline and the second includes all SP samples (Fig. 7c). Fold- and tilt-test results are negative indicating that the magnetization is post folding. When all SP samples are considered together, the average direction is Dec./Inc. = 138.3°/12.7° (Table 1; Fig. 8). However, individual data points scatter significantly in declination (98°–173°); the data as a whole shows an elongated VGP distribution at E–W coordinates (Fig. 8).

DB samples show a single polarity ChRM, with declinations between 345° and 0° and inclination of ∼ 49° (Table 1; Fig. 9) in geographic coordinates. Both sites share a common true direction following both McFadden

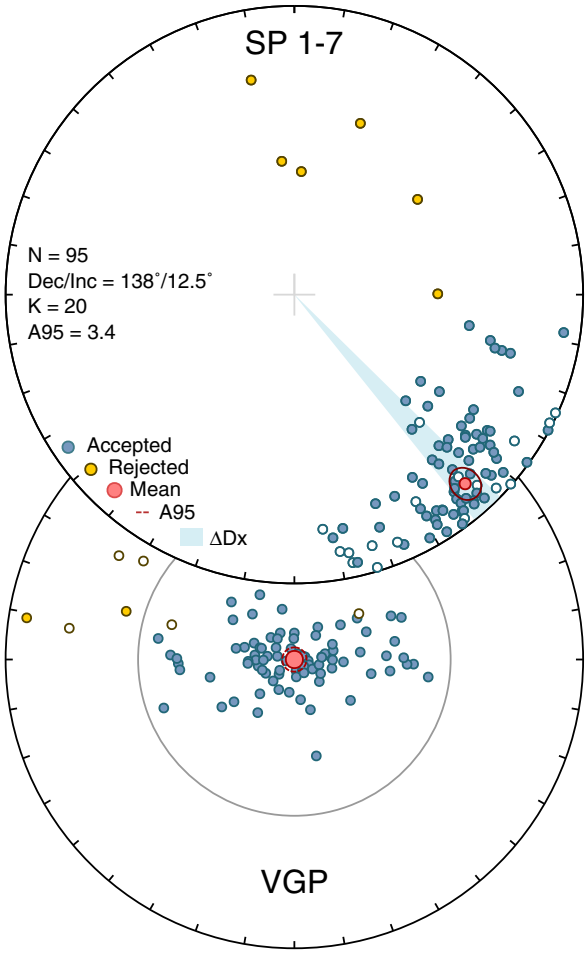

Fig. 8 Equal area projection of all directions obtained from SP samples including their mean direction and projected A95 and ΔDeclination (DDx). Closed (open) points represent the projection on the lower (upper) hemispheres. Below the virtual geomagnetic pole (VGP) projection. Note its elongation in the E–W coordinates

and McElhinny (1990; classification C) and Tauxe (2010) (Supplementary file SF2). After tilt correction directions scatter (Fig. 9) and stop sharing a common true direction (Supplementary file SF2) indicating that samples DB were remagnetized after folding.

3.2 Rock magnetism

3.2.1 Thermomagnetic runs

Nine high-field thermomagnetic runs were measured in air with an in-house-built horizontal translation-type Curie balance with a sensitivity of approximately 5×10^{-9} Am^2 (Mullender et al. 1993). About 50–80 mg of powdered sample material from representative lithologies were placed into quartz glass sample holders and were held in place by quartz wool. Heating and cooling rates were 6 and 10 °C min^{-1} respectively. Stepwise thermomagnetic runs were carried out with intermittent cooling between successive heating steps. The successive heating and cooling segments were 150, 100, 250, 200, 400, 350, 520, 450, 620, 550, 700 and finally back to 25 °C, respectively. Heating and cooling rates were 6 and 10 °C min^{-1} respectively.

Nearly all samples only show a paramagnetic contribution (Fig. 5; Supplementary file SF2). SP1 marks the presence of pyrite and SP2 reveals hematite as main magnetic carrier (Fig. 5). However, stepwise demagnetization diagrams of the natural remanent magnetization (NRM) with a maximum unblocking temperature of ~ 320 °C but high coercitivity (essentially no demagnetization at 100 mT) for several specimens in limestone bearing sites SP1, SP3, SP5–SP7, reveal the presence of pyrrhotite (Fig. 5 and Supplementary file SF2; e.g. Dekkers 1988; Pastor-Galán et al. 2016). Pyrrhotite occurs commonly as a secondary mineral in high-diagenetic and very

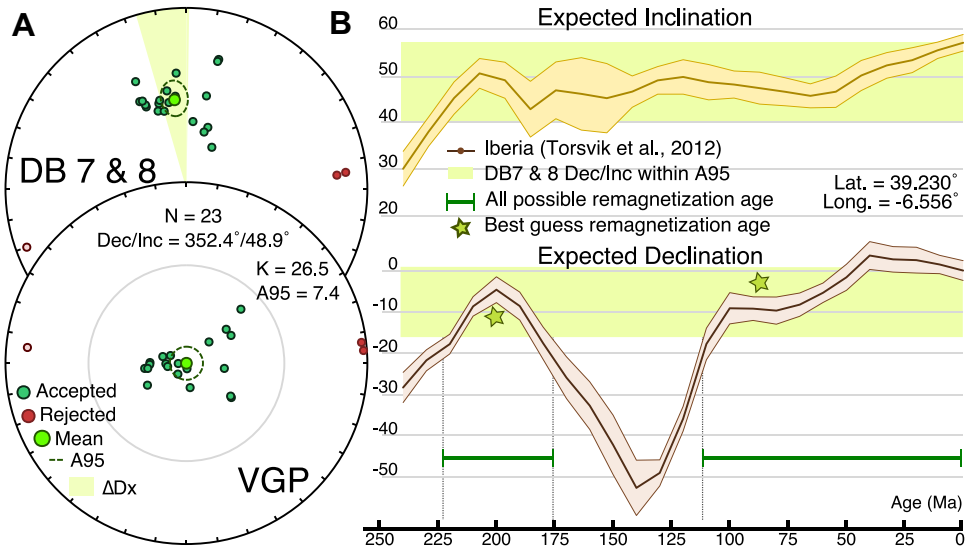

Fig. 9 **a** Equal area projection of DB samples including their mean direction and projected A95 and ΔDeclination. Closed (open) points represent the projection on the lower (upper) hemispheres. Below the virtual geomagnetic pole (VGP) projection. **b** Observed inclination and declination in DB samples compared to the GAPWaP (Torsvik et al. 2012) calculated for the Iberian peninsula (Koymans et al. 2016)

low-grade metamorphic limestones (e.g. Appel et al. 2012; Aubourg et al. 2012). The same diagrams for sites DB7, DB8 and SP4 show the presence of magnetite (maximun unblocking temperature of ~ 580 °C; Fig. 5 and Supplementary file SF2).

3.2.2 Hysteresis loops

We measured seven hysteresis loops (at room temperature) with an alternating gradient force magnetometer (MicroMag Model 2900 with 2 T magnet, Princeton Measurements Corporation, noise level 2×10^{-9} Am^2, P1 phenolic probe). Typical sample mass ranged 20–50 mg. The maximum applied field was 1 T, field increment 10 mT, and the averaging time for each measurement was 0.15 s. The saturation magnetization (Ms), remanent saturation magnetization (Mrs), and coercive force (Bc) were determined from the hysteresis loops. These parameters were determined after correction for the paramagnetic contribution from fields upward of 700 mT. The maximum applied field was 1 T.

Different loop shapes were found (Fig. 10; raw data in SF3): (i) A goose-necked loop that does not saturate at 1 T which points to the presence either of two magnetic minerals or two particle-size distributions with distinct coercivity windows (Fig. 10, SP2.5—red siltstone) indicating the presence of a very hard and a softer phase. (ii) A classical pseudo-single domain loop (Fig. 10, SP4.8—volcanic rock), that saturates before 0.5 T indicating magnetite. (iii) Wasp-waisted loops that barely saturate at 1 T indicating two distinct coercivity windows (Fig. 10, SP7.5—limestone). This points to the presence of a hard phase (pyrrhotite) along with a soft phase (probably magnetite).

3.2.3 IRM acquisition curves

We have obtained 22 isothermal remanent magnetization (IRM) curves from samples of SP1–SP3 and SP5–SP7. Before the actual IRM acquisition, samples were AF demagnetized with the static 3-axis AF protocol with the final demagnetization axis parallel to the subsequent IRM acquisition field, a procedure that generates IRM acquisition curves with a shape as close to a cumulative-lognormal distribution as possible (Egli 2004; Heslop et al. 2004). IRM acquisition curves consist of 61 IRM levels up to 700 mT. IRM acquisition curves show three shapes (Fig. 11a): (1) SP2 samples (red siltstones) that do not saturate at 700 mT; (2) silicified limestones (SP3 and 5) with almost linear IRM acquisition curves; and (3) limestones (SP1, SP3, SP6, SP7) in which most IRM is acquired below 100 mT.

Measured IRM acquisition curves can be decomposed into one or more cumulative log-normal coercivity components representing individual magnetic mineral phases. IRM

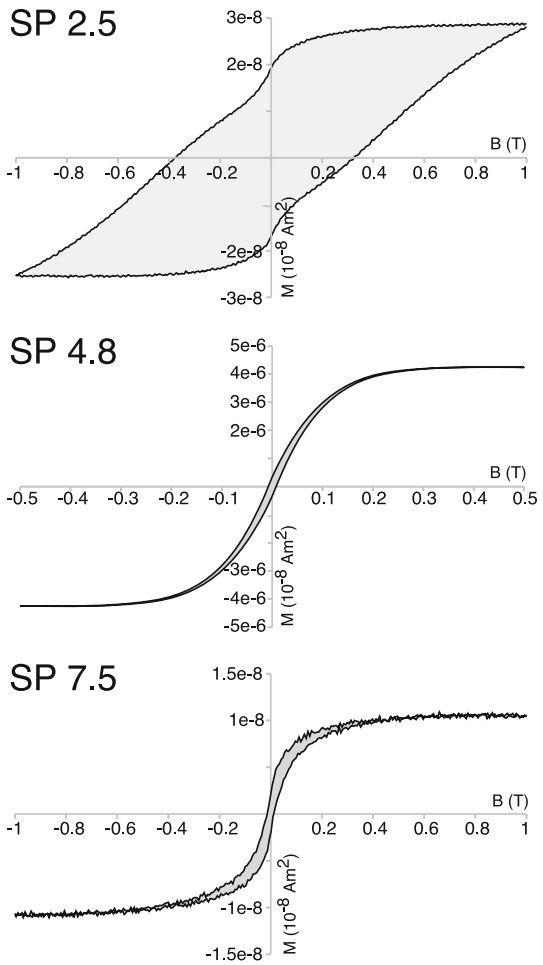

Fig. 10 Typical hysteresis loops. (SP2.5) Goose-necked loop in red siltstones indicating either the presence of two magnetic carriers or two distinct particle-size distributions. (SP4.8) Classical magnetite pseudo-single-domain loop. (SP7.5) Wasp-waisted loop indicating the presence of a hard (pyrrhotite) and a soft phase (probably magnetite)

component analysis enables a semi-quantitative evaluation of different coercivity components (i.e. magnetic minerals or particle sizes) to a measured IRM acquisition curve. Every fitted log-normal curve is characterized by three parameters: (1) The field ($B_{1/2}$) corresponding to the field at which half of the saturation isothermal remanent magnetization (SIRM) is reached; (2) the magnitude of the phase (Mri), which indicates the contribution of the component to the bulk IRM acquisition curve; and (3) The dispersion parameter (DP), expressing the width of the coercivity distribution of that mineral phase and corresponding to one standard deviation of the log-normal function (Kruiver et al. 2001; Heslop et al. 2002).

We analyzed the specimens following the cumulative log-Gaussian approach (Kruiver et al. 2001) with the possibility of including skewness using the online tool MAX UnMix (Maxbauer et al. 2016). SP2 samples are characterized by a single IRM component that does not saturate at

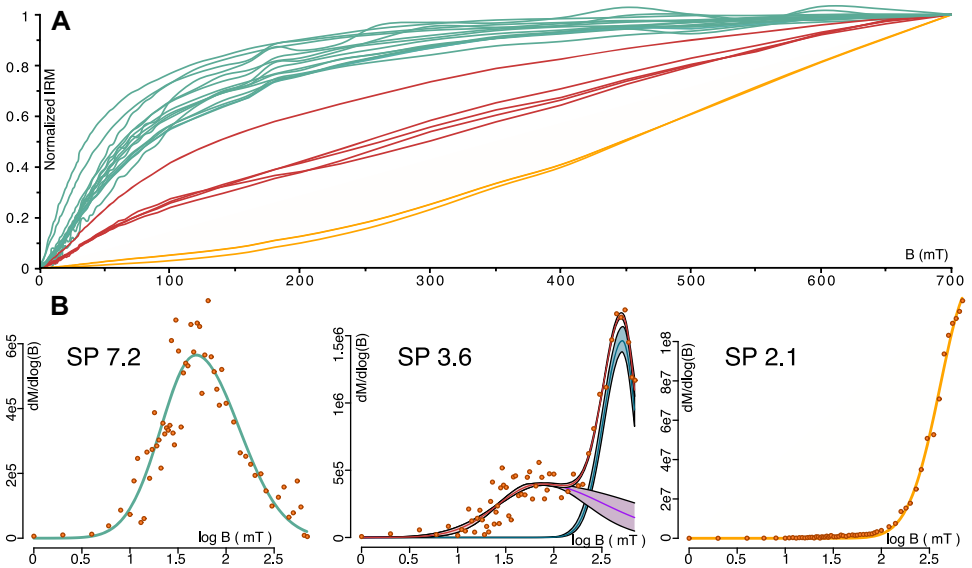

Fig. 11 **a** IRM acquisition curves for selected SP samples, we distinguish three different groups of curve shapes. In yellow samples from SP2 (red siltsones) which do not saturate at 700 mT. In red samples that start to approach saturation, with hard pyrrhotite as main carrier. In green, samples that contains different amounts of pyrrhotite and magnetite. **b** IRM component fitting of the three representative examples of the IRM acquisition curves. The components and uncertainties are marked with different lines. Uncertainties are based on 200 bootstraps. The sum of components colors correspond with those in **a**

700 mT, it has a high $B_{1/2}$ that we have estimated at ~ 1000 mT, and a DP between 0.3 and 0.35 (log units) (Fig. 11b and Supplementary Data). This component indicates hematite as the magnetic mineral. Results from the limestone samples (SP1, SP3, SP5, SP6 and SP7) are characterized by two main IRM components: (a) a component with $B_{1/2}$ between 22 and 90 mT and DP of ~ 0.35 (log units); and (b) a second, higher coercitivity component with a $B_{1/2}$ ranging between 180 and 600 mT and DP between 0.33 and 0.38 (log units). Component 1 is present in all samples and its SIRM percentages vary from 20 to ~ 100% (Fig. 11a). Component 2 therefore ranges from 0% to a maximum of ~ 80% of the SIRM. Component 1 fits with fine-grained magnetite and component 2 is likely to be pyrrhotite (Fig. 11b and Supplementary file SF3). The rock magnetic properties served to chart potential variability of the sample collection and to constrain the NRM interpretation. IRM acquisition curves and hysteresis loops fit nicely with a pyrrothite-magnetite magnetic carrier for limestones and hematite for the sandstones. Presence of pyrrhotite excludes a primary NRM (see Sect. 4) being this an important criterion for our geological interpretation of the NRM directions.

4 Discussion

Rock magnetic analyses indicate pyrrhotite and magnetite to be the magnetic carriers in the limestones whereas magnetite and hematite are the carriers in volcanics, dolomites and siltstones respectively. Pyrrhotite is a secondary mineral which is formed in limestones under anchimetamorphic or very low grade metamorphic conditions. Importantly it is quite stable in low-grade metamorphic rocks under reducing conditions (Aubourg et al. 2012). Pyrrhotite occurs commonly as a magnetic carrier in remagnetized limestone formations in the hinterland of the Iberian Variscan belt (Pastor-Galán et al. 2015a, 2016; Fernández-Lozano et al. 2016). The mere observation of pyrrhotite in limestones points to remagnetized rocks. The known plate tectonic motion of Iberia allows to further constrain the possible remagnetization timing of the studied samples. According to data available, present-day Iberian peninsula was located at low latitude in the southern hemisphere during the late Carboniferous (e.g. Pastor-Galán et al. 2016), crossed the equator during early Permian times (e.g. Weil et al. 2010) and migrated North during the Triassic and Jurassic (e.g. Torsvik et al. 2012). It remained at ~ 30°N until Eocene times, only to head North again until its present day latitude (~ 40°) after the Eocene.

4.1 Significance of Cáceres syncline results (DB samples)

The Cáceres syncline samples (DB7 and DB8) cluster better before any tilt correction with a downward inclination of ~ 49° ± 8.5° (Table 1). Therefore, rocks acquired their remagnetized NRM after the Variscan folding event and during a period in which Iberia was located between

23°N and 38°N. With these inclinations, the global apparent polar wander path (GAPWaP) of Torsvik et al. (2012) calculated for Iberia (using the online application Paleomagnetism.org, cf. Koymans et al. 2016) do not allow the remagnetization to be older than 225 Ma (Fig. 9). The declinations can also be used to further constrain the timing of the remagnetization because significant local Alpine rotations do not occur in the area. In this way the period between 175 Ma and 110 Ma can be discarded (Fig. 9). Our results support a best fit for the remagnetization either at the Triassic–Jurassic boundary interval (210–190 Ma), or during Late Cretaceous (Fig. 9). A very young, subrecent remagnetization, however, cannot be ruled out with our paleomagnetic data. The single normal polarity of the ChRM in the DB samples may be indicative that remagnetization occurred during the Cretaceous superchron (85–126 Ma).

4.2 Sierra de San Pedro, La Codosera-Puebla de Obando and La Roca de la Sierra (SP samples)

In all SP samples, and regardless of their age and lithology, we have documented post-folding magnetizations with shallow inclinations together with the occurrence of a single polarity (Figs. 6, 8). This constrains the samples' NRM acquisition to a period during the Kiaman reversed superchron (318–265 Ma; Langereis et al. 2010) but before Iberia migrated to the northern hemisphere in the early Permian (Weil et al. 2010), hemisphere in which, during reverse chrons, inclinations are upwards. In addition, the average declination shows a general counter-clockwise rotation of $\sim 20°$ from the expected direction at early Permian times (Dec./Inc. = 158°/− 5°; Weil et al. 2010; Table 1), although the rotation varies between sites ranging from 0° to 40° (Table 1). This variability in declination comes with consistent inclinations among the sites.

4.3 Remagnetization in the Variscan hinterland during the Cantabrian orocline formation

When considering all SP results together they are charachterized by largely varying SE declinations (98° to 173°) and an EW elongated VGP distribution (Fig. 8). Samples magnetized at low latitudes are typified by large scatter in inclination and rather small in declination (Tauxe and Kent 2004) in contrast to the distribution found in SP samples. Typical candidates producing elongated VGPs are: (i) structural complexity, (ii) inclination shallowing, or (iii) vertical axis rotations. The studied area is dominated by a relatively simple structure, depicting open upright folds with no plunging axis (see Sect. 2). We can, therefore, discard structural complexity as the main source of scatter. The NRM, being remagnetized after diagenesis and rock consolidation cannot show compaction-related inclination shallowing. Vertical axis rotation is therefore the only plausible cause for the observed scatter.

Pastor-Galán et al. (2015a, 2016) interpreted the dispersion in declination and elongated VGP distribution in other areas of the Central Iberian zone as the result of a remagnetization event taking place during a counter-clockwise rotation related to the formation of the Cantabrian Orocline (310–297 Ma). To further test this hypothesis, we add to the original analysis (Pastor-Galán et al. 2015a) our new dataset from Sierra de San Pedro and data published by Fernández-Lozano et al. (2016), both from the hinterland of the Iberian Variscides (Fig. 12).

It is known that western Iberia registered no major differential rotations since the early Permian (Osete et al. 1997; Neres et al. 2013). Thus, we can calculate the expected declination for each locality at early Permian times using the pole obtained by Weil et al. (2010; Fig. 12). To calculate the expected declination in the late Carboniferous we used the Bootstrapped Orocline test applied to the Cantabrian zone (Pastor-Galán et al. 2017). The orocline test indicates the degree of differential vertical axis rotations underwent by distinctly trending orogenic tracts. When plotting declination vs. strike, the slope between declination and strike is 1 when all curvature is produced by vertical axis rotation; it is 0 when the observed curvature is not due to oroclinal bending (Schwartz and van der Voo 1983; Yonkee and Weil 2010; Pastor-Galán et al. 2017). Once an orocline test is built on a wealth of data, as is the case with the Cantabrian orocline test (Weil et al. 2013), it is possible to infer the expected declination in a portion of the orocline knowing its strike (Fig. 12). Following this procedure we calculated a pre-Cantabrian Orocline formation reference declination and uncertainty for each locality based on their regional strike (using fold axes orientations), assuming that the sites are part of the southern limb of the Cantabrian orocline (Fig. 12) as dictated by the sense of the rotation determined in this study and by Pastor-Galán et al. (2015a, 2016).

Individual or grouped directions from the five localities plot in a girdle from the expected declinations in the late Carboniferous to the early Permian with minor variations in inclination (Fig. 12). This result supports a widespread remagnetization in the hinterland of the Variscan belt in Iberia during the formation of the Cantabrian orocline (Figs. 12, 13). Coeval with the remagnetization a large volume of igneous rocks intruded along the entire hinterland of the Variscan belt in Iberia (e.g. Gutiérrez-Alonso et al. 2011a). Pastor-Galán et al. (2016) ascribed the remagetization in the Tamames syncline (Fig. 12) to the fluids associated with the emplacement of late Carboniferous granitoids in the surrounding area. The results

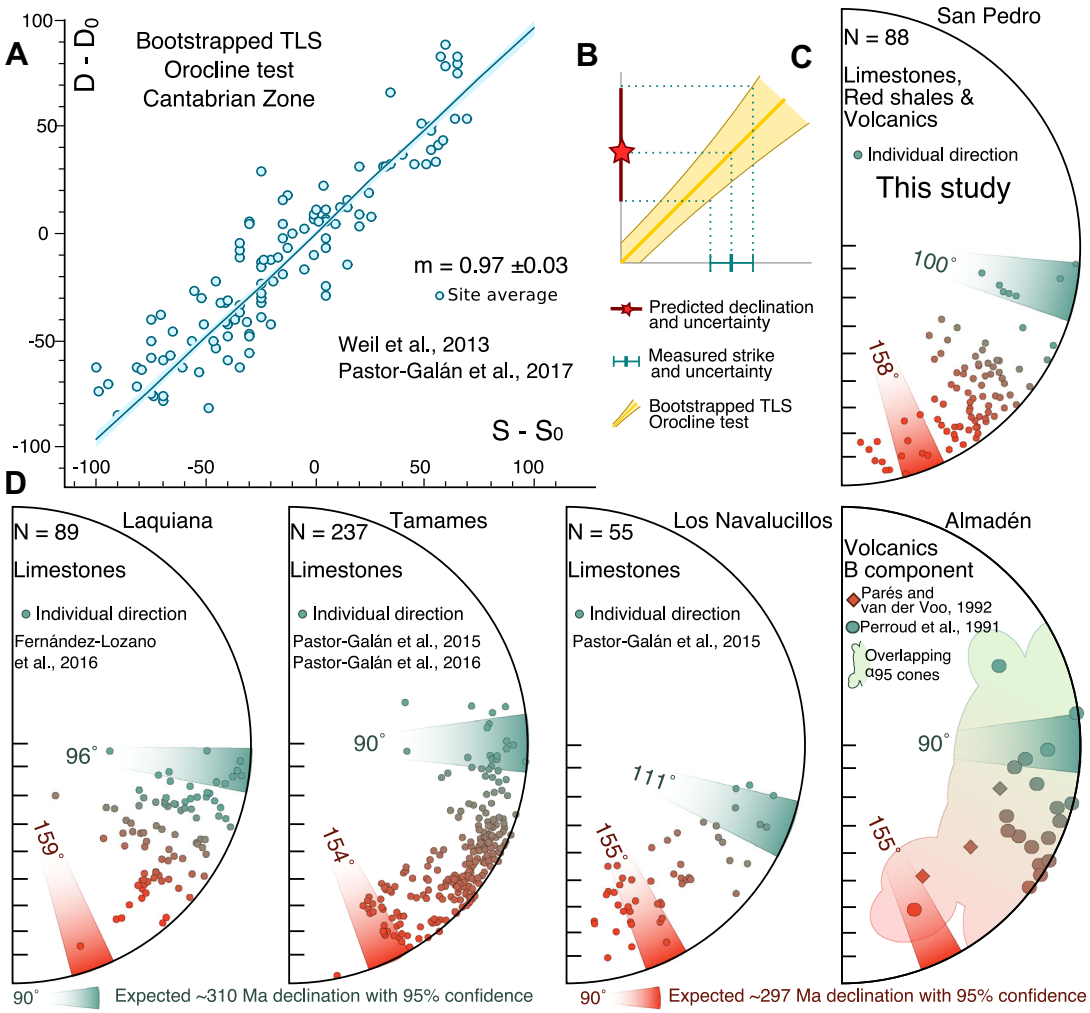

Fig. 12 **a** Bootstrapped orocline test for the Cantabrian orocline, D indicates declination and S orogen strike; D_0 and S_0 are a reference declination and inclination (Pastor-Galán et al. 2017). **b** Methodology to predict the expected declination and uncertainty given an orogen strike. **c** Results from SP samples. Green parachute represent the expected declination for this area if it was part of the southern limb of the Cantabrian orocline. Red parachute respresents the expected declination after the formation of the Cantabrian orocline. **d** Compilation of results in the hinterland of the Iberian Variscides, codes are the same as in **c**

presented in this paper permit us to expand this scenario to the whole Variscan hinterland (Fig. 13).

The paleomagnetic results in the hinterland, in the northern limb, hinge and southern limb of the putative Central Iberian curvature (which is sometimes alleged as an orocline) are identical and show counter-clockwise rotations, which are the expected result for the southern limb of the Cantabrian Orocline (Figs. 12, 13). The lack of differential axis rotations in West and South West Iberia (Figs. 12, 13) fully discards a late Carboniferous or younger origin for the Central Iberian curvature. The latter together with the absence of non-coaxial deformation in the hinge of the Central Iberian bend strongly supports the idea that most of the observed curvature is inherited or a geometrical effect possibly owing to the shape of the Galicia-Tras-os-Montes thrust sheet.

5 Conclusions

Our data from Extremadura (southern Central Iberian zone) show that the rocks in the region were affected by two different remagnetization events localized in two different sectors. The intensely dolomitized limestones from the Cáceres syncline (sites DB7 and DB8), were remagnetized at middle latitudes and their ChRM, carried by magnetite, supports a Mesozoic or Cenozoic remagnetization, being the Triassic-Jurassic boundary interval or the late Cretaceous our best options. The remainder of the studied rocks from Sierra de San Pedro and La Codosera-Puebla de Obando synclines show consistent shallow inclinations and a large scatter in declinations supporting a 70° to 90° CCW rotation. The limestones (sites SP1, SP3, SP5–SP7) show pyrrhotite as one of the magnetic carriers in contrast to the rocks from the Cáceres syncline. The scatter in declination

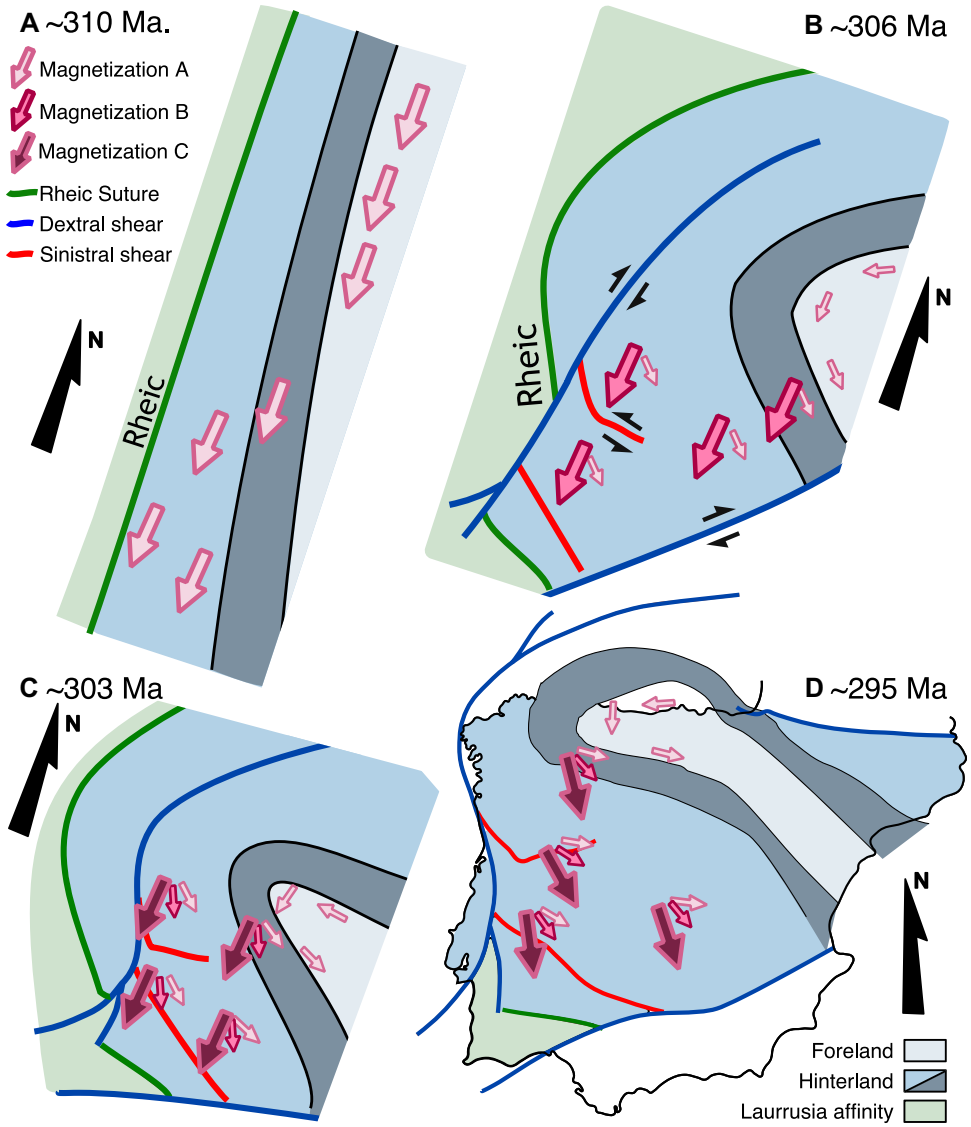

Fig. 13 Cartoon illustrating the extent of the Cantabrian orocline and the remagnetization event in the hinterland during the orocline buckling process

and pyrrhotite as magnetic carrier in limestones are common features in rocks of the Iberian hinterland of the Variscan orogen. We interpret that most of this hinterland remagnetized during the vertical axis rotation that led to the Cantabrian Orocline. The described CCW is common both in the north and south of the putative Central Iberian curve, discarding a late Carboniferous orocline formation in Central Iberia. In contrast, this CCW rotation is fully compatible with the southern limb of the Cantabrian orocline, extending the southern Cantabrian orocline boundaries to at least most of the Iberian peninsula.

Acknowledgements We thank Alicia López-Carmona, Piedad Franco and Eva Manchado for their assistance with thin sections. M. Suárez provided X-Ray diffraction analysis for some of the studied samples. Daniël Brouwer helped to collect and analyze the DB samples. We thank two anonymous reviewers their insights and help to improve this paper. DPG is funded by a Japan Society for Promotion of Science (JSPS) fellowship for overseas researchers (P16329) and a MEXT/JSPS KAKENHI Grant (JP16F16329). GGA is funded by the Spanish Ministry of Economy and Competitiveness under the project ODRE III-Oroclines and Delamination: Relations and Effects (CGL2013-46061-P) and project Origin, metallogeny, climatic effects and cyclicity of Large Igneous Provinces (LIPs)(№ 14.Y26.31.0012) funded by the Russian Federation. DPG wants to acknowledge Billy Shears on its 50th anniversary for this 20 years of raising my smile. This paper is part of UNESCO IGCP Projects 574: Buckling and Bent Orogens, and Continental Ribbons; 597: Amalgamation and breakup of Pangaea: The Type Example of the Supercontinent Cycle; and 648: Supercontinent Cycles and Global Geodynamics.

References

Aerden, D. (2004). Correlating deformation in Variscan NW-Iberia using porphyroblasts; implications for the Ibero-Armorican Arc. *Journal of Structural Geology, 26*(1), 177–196.

Appel, E., Crouzet, C., & Schill, E. (2012). Pyrrhotite remagnetizations in the Himalaya: A review. *Geological Society, London,*

Special Publications, 371(1), 163–180. https://doi.org/10.1144/SP371.1.

Aubourg, C., Pozzi, J.-P., & Kars, M. (2012). Burial, claystones remagnetization and some consequences for magnetostratigraphy. *Geological Society, London, Special Publications, 371*(1), 181–188. https://doi.org/10.1144/SP371.4.

Azor, A., González Lodeiro, F., & Simancas, J. F. (1994). Tectonic evolution of the boundary between the Central Iberian and Ossa-Morena zones (Variscan belt, southwest Spain). *Tectonics, 13,* 45–61.

Ballèvre, M., Martínez Catalán, J. R., López-Carmona, A., Pitra, P., Abati, J., Díez Fernández, R., et al. (2014). Correlation of the nappe stack in the Ibero-Armorican arc across the Bay of Biscay: A joint French-Spanish project. In K. Schulmann, J. M. Lardeaux, V. Janousek, & G. Oggiano (Eds.), *The Variscan orogeny: Extent, timescale and the formation of the European crust* (pp. 77–113). London: Geological Society of London, Special Publication 405.

Barreiro, J. G., Wijbrans, J. R., Castineiras, P., Catalan, J. R. M., Arenas, R., Garcia, F. D., et al. (2006). Ar-40/Ar-39 laserprobe dating of mylonitic fabrics in a polyorogenic terrane of NW Iberia. *Journal of the Geological Society, 163,* 61–73.

Bea, F., Montero, P. G., Gonzalez-Lodeiro, F., Talavera, C., Molina, J. F., Scarrow, J. H., et al. (2006). Zircon thermometry and U-Pb ion-microprobe dating of the gabbros and associated migmatites of the Variscan Toledo anatectic complex, Central Iberia. *Journal of the Geological Society, 163,* 847–855.

Bochmann, H.G. (1956). *Stratigraphie und tektonik der zentralen Extremadura in Bereich von Cáceres und der östliche Sierra de San Pedro (Spanien)*. Unveröff. Dies. Match. Naturviss. Fak. Univ. Münster. p. 195 (Unpublished).

Calvín, P., Casas-Sainz, A. M., Villalaín, J. J., & Moussaid, B. (2017). Diachronous folding and cleavage in an intraplate setting (Central High Atlas, Morocco) determined through the study of remagnetizations. *Journal of Structural Geology, 97,* 144–160. https://doi.org/10.1016/j.jsg.2017.02.009.

Castiñeiras, P., Villaseca, C., Barbero, L., & Romera, C. M. (2008). SHRIMP U-Pb zircon dating of anatexis in high-grade migmatite complexes of Central Spain: Implications in the Hercynian evolution of Central Iberia. *International Journal of Earth Sciences, 97,* 35–50.

Clariana García, M.P., Rubio Pascual, F., Montes Santiago, M.J., & González Clavijo, E.J. (2017). Mapa Geológico Digital cóntinuo E. 1: 50.000, Zona Centroibérica. Domino esquisto-grauváquico y Cuenca del Guadiana (Zona-1400). In GEODE. Mapa Geológico Digital continuo de España. (online). Retrived Apr 01, 2017 from http://info.igme.es/cartografiadigital/geologica/geodezona.aspx?Id=Z1400.

Corretgé, L. G., Suárez, O., & Tena, M. (1982). Los granitos, rocas volcánicas y rocas volcanoclásticas del Sinclinal de Cáceres. *Trabajos de Geología, Universidad de Oviedo, 12,* 251–271.

Dallmeyer, R. D., & Ibarguchi, J. I. G. (1990). Age of amphibolitic metamorphism in the ophiolitic unit of the Morais allochthon (Portugal): Implications for early Hercynian orogenesis in the Iberian Massif. *Journal of the Geological Society, 147,* 873–878.

Dallmeyer, R. D., Martínez Catalán, J. R., Arenas, R., Gil Ibarguchi, J. I., Gutiérrez-Alonso, G., Farias, P., et al. (1997). Diachronous Variscan tectonothermal activity in the NW Iberian Massif: Evidence from 40Ar/39Ar dating of regional fabrics. *Tectonophysics, 277*(4), 307–337. https://doi.org/10.1016/S0040-1951(97)00035-8.

Dekkers, M. J. (1988). Magnetic properties of natural pyrrhotite part I: Behaviour of initial susceptibility and saturation-magnetization-related rock-magnetic parameters in a grain-size dependent framework. *Physics of the Earth and Planetary Interiors, 52*(3–4), 376–393. https://doi.org/10.1016/0031-9201(88)90129-X.

Deenen, M. H., Langereis, C. G., van Hinsbergen, D. J. & Biggin, A. J. (2011). Geomagnetic secular variation and the statistics of palaeomagnetic directions. *Geophysical Journal International, 186*(2), 509–520.

Dunn, A. M., Reynolds, P. H., Clarke, D. B., & Ugidos, J. M. (1998). A comparison of the age and composition of the Shelburne dyke, Nova Scotia, and the Messejana dyke, Spain. *Canadian Journal of Earth Sciences, 35,* 1110–1115.

Egli, R. (2004). Characterization of individual rock magnetic components by analysis of remanence curves. *Physics and Chemistry of the Earth, 29*(13–14 SPEC. ISS.), 851–867. https://doi.org/10.1016/j.pce.2004.04.001.

Elmore, R. D., Muxworthy, A. R., & Aldana, M. (2012). Remagnetization and chemical alteration of sedimentary rocks. *Geological Society, London, Special Publications, 371*(1), 1–21.

Enkin, R. J., Osadetz, K. G., Baker, J., & Kisilevsky, D. (2000). Orogenic remagnetizations in the front ranges and inner foothills of the southern Canadian Cordillera: Chemical harbinger and thermal handmaiden of Cordilleran deformation. *Geological Society of America Bulletin, 112*(6), 929–942. https://doi.org/10.1130/0016-7606(2000)112<929:ORITFR>2.0.CO;2.

Fernández-Lozano, J., Pastor-Galán, D., Gutiérrez-Alonso, G., & Franco, P. (2016). New kinematic constraints on the Cantabrian orocline: A paleomagnetic study from the Peñalba and Truchas synclines, NW Spain. *Tectonophysics, 681,* 195–208. https://doi.org/10.1016/j.tecto.2016.02.019.

Fernandez-Suarez, J., Corfu, F., Arenas, R., Marcos, A., Martínez Catalan, J. R., Garcia, F. D., et al. (2002). U-Pb evidence for a polyorogenic evolution of the HP-HT units of the NW Iberian Massif. *Contributions to Mineralogy and Petrology, 143*(2), 236–253.

Franke, W. (1989). Variscan plate tectonics in Central Europe—current ideas and open questions. *Tectonophysics, 169*(4), 221–228. https://doi.org/10.1016/0040-1951(89)90088-7.

Gong, Z., Dekkers, M. J., Heslop, D., & Mullender, T. A. T. (2009). End-member modelling of isothermal remanent magnetization (IRM) acquisition curves: A novel approach to diagnose remagnetization. *Geophysical Journal International, 178*(2), 693–701. https://doi.org/10.1111/j.1365-246X.2009.04220.x.

Gutiérrez-Alonso, G., Collins, A. S., Fernández-Suárez, J., Pastor-Galán, D., González-Clavijo, E., Jourdan, F., et al. (2015a). Dating of lithospheric buckling: 40Ar/39Ar ages of syn-orocline strike-slip shear zones in northwestern Iberia. *Tectonophysics*. https://doi.org/10.1016/j.tecto.2014.12.009.

Gutiérrez-Alonso, G., Fernández-Suárez, J., Jeffries, T. E., Johnston, S. T., Pastor-Galán, D., Murphy, J. B., et al. (2011a). Diachronous post-orogenic magmatism within a developing orocline in Iberia, European Variscides. *Tectonics*. https://doi.org/10.1029/2010TC002845.

Gutiérrez-Alonso, G., Fernández-Suárez, J., Pastor-Galán, D., Johnston, S. T., Linnemann, U., Hofmann, M., et al. (2015b). Significance of detrital zircons in Siluro-Devonian rocks from Iberia. *Journal of the Geological Society, 172*(3), 309–322.

Gutiérrez-Alonso, G., Fernández-Suárez, J., & Weil, A. B. (2004). Orocline triggered lithospheric delamination. In A. B. Weil & A. Sussman (Eds.), *Orogenic curvature: Integrating paleomagnetic and structural analyses* (Vol. 383, pp. 121–131). Boulder: Geological Society of America, GSA Special Papers. https://doi.org/10.1130/0-8137-2383-3(2004)383[121:OTLD]2.0.CO;2.

Gutiérrez-Alonso, G., Johnston, S. T., Weil, A. B., Pastor-Galán, D., & Fernández-Suárez, J. (2012). Buckling an orogen: The Cantabrian Orocline. *GSA Today, 22*(7), 4–9.

Gutiérrez-Alonso, G., Murphy, J. B., Fernández-Suárez, J., Weil, A. B., Franco, M. P., & Gonzalo, J. C. (2011b). Lithospheric

delamination in the core of Pangea: Sm-Nd insights from the Iberian mantle. *Geology, 39*(2), 155–158. https://doi.org/10.1130/G31468.1.

Heslop, D., Dekkers, M. J., Kruiver, P. P., & Van Oorschot, I. H. M. (2002). Analysis of isothermal remanent magnetization acquisition curves using the expectation-maximization algorithm. *Geophysical Journal International, 148*(1), 58–64. https://doi.org/10.1046/j.0956-540x.2001.01558.x.

Heslop, D., McIntosh, G., & Dekkers, M. J. (2004). Using time- and temperature-dependent Preisach models to investigate the limitations of modelling isothermal remanent magnetization acquisition curves with cumulative log Gaussian functions. *Geophysical Journal International, 157*(1), 55–63. https://doi.org/10.1111/j.1365-246X.2004.02155.x.

Hirt, A. M., Lowrie, W., Julivert, M., & Arboleya, M. L. (1992). Paleomagnetic results in support of a model for the origin of the Asturian arc. *Tectonophysics, 213*(3–4), 321–339.

Huang, W., Lippert, P. C., Zhang, Y., Jackson, M. J., Dekkers, M. J., Li, J., et al. (2017). Remagnetization of carbonate rocks in southern Tibet: Perspectives from rock magnetic and petrographic investigations. *Journal of Geophysical Research: Solid Earth, 122*(4), 2434–2456. https://doi.org/10.1002/2017JB013987.

Izquierdo-Llavall, E., Sainz, A. C., Oliva-Urcia, B., Burmester, R., Pueyo, E. L., & Housen, B. (2015). Multi-episodic remagnetization related to deformation in the Pyrenean Internal Sierras. *Geophysical Journal International, 201*(2), 891–914. https://doi.org/10.1093/gji/ggv042.

Julivert, M. (1971). Décollement tectonics in the Hercynian cordillera of NW Spain. *American Journal of Science, 270,* 1–29.

Koymans, M. R., Langereis, C. G., Pastor-Galán, D. & van Hinsbergen, D. J. (2016). Paleomagnetism. org: An online multi-platform open source environment for paleomagnetic data analysis. *Computers and Geosciences*, *93*, 127–137.

Kruiver, P. P., Dekkers, M. J., & Heslop, D. (2001). Quantification of magnetic coercivity components by the analysis of acquisition curves of isothermal remanent magnetisation. *Earth and Planetary Science Letters, 189*(3–4), 269–276. https://doi.org/10.1016/S0012-821X(01)00367-3.

Langereis, C. G., Krijgsman, W., Muttoni, G., & Menning, M. (2010). Magnetostratigraphy—concepts, definitions, and applications. *Newsletters on Stratigraphy, 43*(3), 207–233. https://doi.org/10.1127/0078-0421/2010/0043-0207.

López Díaz, F. (1991). Características de la primera fase (distensiva) hercínica en la Sierra de San Pedro (Cáceres-Badajoz). *Cuadernos del Laoratorio Xeolóxico de Laxe, 16,* 53–63.

López-Moro, F. J., Murciego, A. & López-Plaza, M. (2007). Silurian/Ordovician asymmetrical sill-like bodies from La Codosera syncline, W Spain: a case of tholeiitic partial melts emplaced in a single magma pulse and derived from a metasomatized mantle source. *Lithos*, *96*(3), 567–590.

López-Carmona, A., Abati, J., Pitra, P., & Lee, J. K. W. (2014). Retrogressed lawsonite blueschists from the NW Iberian Massif: P–T–t constraints from thermodynamic modelling and 40Ar/39Ar geochronology. *Contributions to Mineralogy and Petrology, 167*(3), 987. https://doi.org/10.1007/s00410-014-0987-5.

López-Moro, F. J., López-Plaza, M., Gutiérrez-Alonso, G., Fernández-Suárez, J., López-Carmona, A., Hofmann, M., et al. (2017). Crustal melting and recycling: Geochronology and sources of Variscan syn-kinematic anatectic granitoids of the Tormes Dome (Central Iberian zone). AU–Pb LA-ICP-MS study. *International Journal of Earth Sciences*. https://doi.org/10.1007/s00531-017-1483-8.

Lotze, F. (1945). Zur gliederung des Varisciden der Iberischen Meseta. *Geotektonische Forschungen, 6,* 78–92.

Martínez Catalán, J. R. (2011). Are the oroclines of the Variscan belt related to late Variscan strike-slip tectonics? *Terra Nova, 23*(4), 241–247. https://doi.org/10.1111/j.1365-3121.2011.01005.x.

Martínez Catalán, J. R., Aerden, D. G. A. M., & Carreras, J. (2015). The "Castilian bend" of Rudolf Staub (1926): Historical perspective of a forgotten orocline in Central Iberia. *Swiss Journal of Geosciences, 108*(2–3), 289–303. https://doi.org/10.1007/s00015-015-0202-3.

Martínez Catalán, J. R., Arenas, R., Díaz García, F., & Abati, J. (1997). Variscan accretionary complex of northwest Iberia: Terrane correlation and succession of tectonothermal events. *Geology, 25,* 1103–1106.

Martínez Catalán, J. R., Arenas, R., & Díez Balda, M. A. (2003). Large extensional structures developed during emplacement of a crystalline thrust sheet: The Mondoñedo nappe (NW Spain). *Journal of Structural Geology, 25,* 1815–1839.

Martínez Poyatos, D. (2002). *Estructura del borde meridional de la zona Centroibérica y su relación con el contacto entre las zonas Centroibérica y de Ossa-Morena*. Laboratorio Xeolóxico de Laxe, Serie Nova Terra, A Coruña, 18(p. 295). PhD Thesis, Univ. Granada, 1997.

Martínez Poyatos, D., Nieto, F., Azor, A., & Simancas, J. F. (2001). Relationships between very low-grade metamorphism and tectonic deformation: Examples from the southern Central Iberian zone (Iberian massif, Variscan belt). *Journal Geological Society, London, 158,* 953–968.

Matas, J., & Martín Parra, L.M. (2017). Mapa Geológico Digital continuo. 1: 50.000, Dominio de Obejo-Valsequillo de la Zona Centroibérica (Zona 2500). in GEODE. Mapa Geológico Digital continuo de España (online). Retrieved Apr 01, 2017, from http://info.igme.es/cartografiadigital/geologica/geodezona.aspx?Id=Z2500.

Maxbauer, D. P., Feinberg, J. M., & Fox, D. L. (2016). MAX UnMix: A web application for unmixing magnetic coercivity distributions. *Computers & Geosciences, 95,* 140–145. https://doi.org/10.1016/j.cageo.2016.07.009.

Mcfadden, P. L., McElhinny, M. W., & Ri, N. (1990). Classification of the reversal test in palaeomagnetism. *Geophysical Journal International, 103*(3), 725–729. https://doi.org/10.1111/j.1365-246X.1990.tb05683.x.

Merino-Tomé, O. A., Bahamonde, J. R., Colmenero, J. R., Heredia, N., Villa, E., & Farias, P. (2009). Emplacement of the Cuera and Picos de Europa imbricate system at the core of the Iberian-Armorican arc (Cantabrian zone, north Spain): New precisions concerning the timing of arc closure. *Geological Society of America Bulletin, 121*(5–6), 729–751. https://doi.org/10.1130/B26366.1.

Mullender, T. A. T., Frederichs, T., Hilgenfeldt, C., de Groot, L. V., Fabian, K., & Dekkers, M. J. (2016). Automated paleomagnetic and rock magnetic data acquisition with an in-line horizontal "2G" system. *Geochemistry, Geophysics, Geosystems, 17,* 3546–3559. https://doi.org/10.1002/2016GC006436.

Mullender, T. A. T., van Velzen, A. J., & Dekkers, M. J. (1993). Continuous drift correction and separate identification of ferrimagnetic and paramagnetic contributions in thermomagnetic runs. *Geophysical Journal International, 114*(3), 663–672. https://doi.org/10.1111/j.1365-246X.1993.tb06995.x.

Nance, R. D., Gutiérrez-Alonso, G., Keppie, J. D., Linnemann, U., Murphy, J. B., Quesada, C., et al. (2010). Evolution of the Rheic Ocean. *Gondwana Research, 17*(2–3), 194–222. https://doi.org/10.1016/j.gr.2009.08.001.

Neres, M., Miranda, J. M., & Font, E. (2013). Testing Iberian kinematics at Jurassic-Cretaceous times. *Tectonics, 32*(5), 1312–1319. https://doi.org/10.1002/tect.20074.

Osete, M. L., Rey, D., Villalaín, J. J., & Juárez, M. T. (1997). The late Carboniferous to late Triassic segment of the apparent polar

wander path of Iberia. *Geologie En Mijnbouw (Geology and Mining), 76*(1/2), 105–119. https://doi.org/10.1023/A:1003197500052.

Palencia Ortas, A., Osete, M. L., Vegas, R., & Silva, P. (2006). Paleomagnetic study of the Messejana Plasencia dyke (Portugal and Spain): A lower Jurassic paleopole for the Iberian plate. *Tectonophysics, 420,* 455–472.

Parés, J. M., & Van der Voo, R. (1992). Paleozoic paleomagnetism of Almaden, Spain: A cautionary note. *Journal of Geophysical Research, 97*(B6), 9353–9356. https://doi.org/10.1029/91JB03073.

Parra, L. M. M., González Lodeiro, F., Martínez Poyatos, D., & Matas, J. (2006). The Puente Génave-Castelo de Vide Shear zone (southern Central Iberian zone, Iberian Massif): Geometry, kinematics and regional implications. *Bulletin de la Société Géologique de France, 177,* 191–202.

Pastor-Galán, D., Dekkers, M. J., Gutiérrez-Alonso, G., Brouwer, D., Groenewegen, T., Krijgsman, W., et al. (2016). Paleomagnetism of the Central Iberian curve's putative hinge: Too many oroclines in the Iberian Variscides. *Gondwana Research, 39,* 96–113. https://doi.org/10.1016/j.gr.2016.06.016.

Pastor-Galán, D., Groenewegen, T., Brouwer, D., Krijgsman, W., & Dekkers, M. J. (2015a). One or two oroclines in the Variscan orogen of Iberia? Implications for Pangea amalgamation. *Geology, 43*(6), 527–530. https://doi.org/10.1130/G36701.1.

Pastor-Galán, D., Gutiérrez-Alonso, G., & Weil, A. B. (2011). Orocline timing through joint analysis: Insights from the Ibero-Armorican Arc. *Tectonophysics, 507*(1–4), 31–46. https://doi.org/10.1016/j.tecto.2011.05.005.

Pastor-Galan, D., Gutierrez-Alonso, G., Zulauf, G., & Zanella, F. (2012). Analogue modeling of lithospheric-scale orocline buckling: Constraints on the evolution of the Iberian-Armorican Arc. *Geological Society of America Bulletin, 124*(7–8), 1293–1309. https://doi.org/10.1130/B30640.1.

Pastor-Galán, D., Martín-Merino, G., & Corrochano, D. (2014). Timing and structural evolution in the limb of an orocline: The Pisuerga-Carrión Unit (southern limb of the Cantabrian Orocline, NW Spain). *Tectonophysics, 622,* 110–121. https://doi.org/10.1016/j.tecto.2014.03.004.

Pastor-Galán, D., Mulchrone, K. F., Koymans, M. R., van Hinsbergen, D. J., & Langereis, C. G. (2017). Bootstrapped total least squares orocline test: A robust method to quantify vertical-axis rotation patterns in orogens, with examples from the Cantabrian and Aegean oroclines. *Lithosphere, 9*(3), 499–511.

Pastor-Galán, D., Ursem, B., Meere, P. A., & Langereis, C. (2015b). Extending the Cantabrian Orocline to two continents (from Gondwana to Laurussia). Paleomagnetism from South Ireland. *Earth and Planetary Science Letters, 432,* 223–231. https://doi.org/10.1016/j.epsl.2015.10.019.

Perroud, H., Calza, F., & Khattach, D. (1991). Paleomagnetism of the Silurian Volcanism at Almaden, Southern Spain. *Journal of Geophysical Research, 96*(B2), 1949–1962.

Pueyo, E. L., Mauritsch, H. J., Gawlick, H.-J., Scholger, R., & Frisch, W. (2007). New evidence for block and thrust sheet rotations in the central northern Calcareous Alps deduced from two pervasive remagnetization events. *Tectonics*. https://doi.org/10.1029/2006TC001965.

Rincón, P. J., Hermosilla, J., Vegas, R., Pascual, G., Muñoz-Martín, A., & Martínez-Solares, J. M. (2000). Cálculo automático del desplazamiento en un sector del sistema falla-dique de Plasencia. *Geogaceta, 27,* 143–146.

Rodríguez González, R., Medina Varea, P., González Lodeiro, F., Martín Parra, L. M., Martínez Poyatos, D., & Matas, J. (2007). Microflora y conodontos del Mississippiense en la Fm Gévora (núcleo del Sinforme La Codosera-Puebla de Obando, SO de la Zona Centroibérica). *Revista de la Sociedad Geológica de España, 20*(1–2), 71–88.

Rosso de Luna, J., & Hernández Pacheco, F. (1954). *Hoja geológica no 750 (Gallina), 1:50000, 1ª edición* (p. 51). Madrid: I.G.M.E.

Rubio-Ordóñez, A., García-Moreno, O., Montero, P., & Bea, F. (2016). Nuevas aportaciones a la datación cronológica de los granitos de Cabeza de Araya, (Cáceres). *Geo-Temas, 16*(2), 63–66.

Santos, J.A., Apalategui, O., Carvajal, A. & Gracia, J. (1991a). Mapa Geológico de España 1.50.000, hoja no 750 (Botoa). Madrid: IGME.

Santos, J.A., Apalategui, O., Carvajal, A. & Gracia, J. (1991b). Mapa Geológico de España (MAGNA) 1:50.000, hoja no 751 (Villar del Rey) (p. 61). Madrid: IGME.

Santos, J. A., & Casas, J. (1979). Geología del sinclinorio de São Mamede-La Codosera. Zona española (Prov. de Cáceres y Badajoz). *Boletin Geológico y Minero, 90,* 420–431.

Schwartz, S. Y., & Van der Voo, R. (1983). Paleomagnetic evaluation of the orocline hypothesis in the central and southern Appalachians. *Geophysical Research Letters, 10*(7), 505–508.

Shaw, J., Johnston, S. T., & Gutiérrez-Alonso, G. (2016). Orocline formation at the core of Pangea: A structural study of the Cantabrian orocline, NW Iberian Massif. *Lithosphere, 8*(1), 97. https://doi.org/10.1130/L461.1.

Shaw, J., Johnston, S. T., Gutiérrez-Alonso, G., & Weil, A. B. (2012). Oroclines of the Variscan orogen of Iberia: Paleocurrent analysis and paleogeographic implications. *Earth and Planetary Science Letters, 329,* 60–70.

Simancas, J. F., Martínez Poyatos, D., Expósito, I., Azor, A., & González Lodeiro, F. (2001). The structure of a major suture zone in the SW Iberian Massif: The Ossa-Morena/Central Iberian contact. *Tectonophysics, 332,* 295–308.

Solá, A. R., Williams, I. S., Neiva, A. M. R., & Ribeiro, M. L. (2009). U-Th-Pb SHRIMP ages and oxygen isotope composition of zircon from two contrasting late Variscan granitoids, Nisa-Albuquerque batholith, SW Iberian Massif: Petrologic and regional implications. *Lithos, 111*(3–4), 156–167. https://doi.org/10.1016/j.lithos.2009.03.045.

Soldevila Bartolí, J. (1992a). La sucesión Paleozoica en el sinforme de La Codosera-Puebla de Obando (Provincias de Cáceres y Badajoz, SO de España). *Estudios Geológicos, 48,* 353–362.

Soldevila Bartolí, J. (1992b). La sucesión Paleozoica en el sinforme de La Sierra de San Pedro (Provincias de Cáceres y Badajoz, SO de España). *Estudios Geológicos, 48,* 363–379.

Stamatakos, J., Hirt, A. M., & Lowrie, W. (1996). The age and timing of folding in the central Appalachians from paleomagnetic results. *Geological Society of America Bulletin, 108*(7), 815–829. https://doi.org/10.1130/0016-7606(1996)108<0815:TAATOF>2.3.CO;2.

Staub, R. (1926). *Gedanken zur Tektonik Spaniens. Vierteljahrsschrift der Naturforschenden Gesellschaft,* (Vol. 71). Zürich.

Tauxe, L. (2010). *Essentials of paleomagnetism*. Retrieved from https://scholar.google.com/scholar?cluster=6824168530500552 67&hl=en&oi=scholarr#0.

Tauxe, L. & Watson, G. S. (1994). The fold test: an eigen analysis approach. *Earth and Planetary Science Letters*, *122*(3–4), 331–341.

Tauxe, L., & Kent, D. V. (2004). A simplified statistical model for the geomagnetic field and the detection of shallow bias in paleomagnetic inclinations: Was the ancient magnetic field dipolar? *Timescales of the Paleomagnetic field, 1,* 101–115.

Tohver, E., Weil, A. B., Solum, J. G., & Hall, C. M. (2008). Direct dating of carbonate remagnetization by 40Ar/39Ar analysis of the smectite–illite transformation. *Earth and Planetary Science Letters, 274*(3–4), 524–530. https://doi.org/10.1016/j.epsl.2008.08.002.

Torsvik, T. H., van der Voo, R., Preeden, U., Mac Niocaill, C., Steinberger, B., Doubrovine, P. V., et al. (2012). Phanerozoic polar wander, palaeogeography and dynamics. *Earth-Science Reviews, 114*(3–4), 325–368. https://doi.org/10.1016/j.earscirev.2012.06.007.

van der Voo, R., Stamatakos, J. A., & Pares, J. M. (1997). Kinematic constraints on thrust-belt curvature from syndeformational magnetizations in the Lagos del Valle syncline in the Cantabrian Arc, Spain. *Journal of Geophysical Research-Solid Earth, 102*(B5), 10105–10119.

Villamor, P. (2002). *Cinemática terciaria y cuaternaria de la falla de Alentejo-Plasencia y su influencia en la peligrosidad sísmica del interior de La Península Ibérica* (p. 343). Tesis Doctoral: Universidad Complutense de Madrid.

Wallis, R.H. (1983). A lacustrine/deltaic/fluvial/swamp succession from the Stephanian B of Puertollano, Spain. In Lemos de Sousa, M.J. & Wagner, R.H. (Eds.), Papers on the Carboniferous of the Iberian peninsula (sedimentology, stratigraphy, paleontology, tectonics and geochemistry) (pp. 51–67). *Ann. Fac. de Ciências*, Portugal: University of Porto.

Weil, A. B. (2006). Kinematics of orocline tightening in the core of an arc: Paleomagnetic analysis of the Ponga Unit, Cantabrian Arc, northern Spain. *Tectonics*. https://doi.org/10.1029/2005TC001861.

Weil, A. B., Gutiérrez-Alonso, G., & Conan, J. (2010). New time constraints on lithospheric-scale oroclinal bending of the Ibero-Armorican Arc: A palaeomagnetic study of earliest Permian rocks from Iberia. *Journal of the Geological Society, 167*(1), 127–143. https://doi.org/10.1144/0016-76492009-002.

Weil, A. B., Gutiérrez-Alonso, G., Johnston, S. T., & Pastor-Galán, D. (2013). Kinematic constraints on buckling a lithospheric-scale orocline along the northern margin of Gondwana: A geologic synthesis. *Tectonophysics, 582,* 25–49. https://doi.org/10.1016/j.tecto.2012.10.006.

Weil, A. B., & Van der Voo, R. (2002). Insights into the mechanism for orogen-related carbonate remagnetization from growth of authigenic Fe-oxide: A scanning electron microscopy and rock magnetic study of Devonian carbonates from northern Spain. *Journal of Geophysical Research-Solid Earth, 107*(B4), 14.

Weil, A. B., van der Voo, R., & van der Pluijm, B. A. (2001). Oroclinal bending and evidence against the Pangea megashear: The Cantabria-Asturias arc (northern Spain). *Geology, 29*(11), 991–994.

Weil, A. B., Van Der Voo, R., van der Pluijm, B. A., & Parés, J. M. (2000). The formation of an orocline by multiphase deformation: a paleomagnetic investigation of the Cantabria-Asturias Arc (northern Spain). *Journal of Structural Geology, 22*(6), 735–756. https://doi.org/10.1016/S0191-8141(99)00188-1.

Yonkee, A., & Weil, A. B. (2010). Quantifying vertical axis rotation in curved orogens: Correlating multiple data sets with a refined weighted least squares strike test. *Tectonics, 29*(3), 31. https://doi.org/10.1029/2008TC002312.

Zegers, T. E., Dekkers, M. J., & Bailly, S. (2003). Late Carboniferous to Permian remagnetization of Devonian limestones in the Ardennes: Role of temperature, fluids, and deformation. *Journal of Geophysical Research: Solid Earth*. https://doi.org/10.1029/2002JB002213.